ChemPubSoc Europe

DOI: 10.1002/ejoc.201700046

EurJOC European Journal of Organic Chemistry

Full Paper

Substituent Engineering

Effect of Double Branching in α,ω-Substituted Oligothiophenes on Thermal Solid-State Properties

Jochen Gülcher,[a] Roman Vill,[a] Markus Braumüller,[a] Khosrow Rahimi,[b] Wim H. de Jeu,[b] Ahmed Mourran,[b] and Ulrich Ziener*[a]

Abstract: A systematic series of septi-, noni- and undecithiophenes and the corresponding pre-oligomers with five different dendrimer-like branched end-groups have been synthesized and their thermal solid-state properties investigated. The substituents vary in terms of the lengths of the linkers between the silicon branching points. Comparison of the compounds in the series reveals that the linker connecting the oligomeric core with the first branching point has the strongest effect on the thermal properties. Furthermore, the relatively large volume of the substituents causes surprisingly low overall transition enthalpies and entropies for the oligomers of 10–20 kJ mol^{-1} and 15–40 J mol^{-1} K^{-1}, respectively, whereas the pre-oligomers with interrupted conjugation display values in the range of 15–40 kJ mol^{-1} and 40–100 J mol^{-1} K^{-1}, respectively. Polarizing optical microscopy (POM) revealed textures pointing to smectic and columnar liquid-crystalline phases but X-ray and AFM data of a representative example are typical of cubic phases.

Introduction

Semi-conducting organic materials for electronic applications like organic field-effect transistors (OFETs), organic solar cells (OSCs) or organic light-emitting diodes (OLEDs) require a subtle fine-tuning of the intermolecular interactions for efficient charge transport.[1–4] In the past, research activities on electronic organic materials were mostly dedicated to the tailoring of the π functional moieties and extending the conjugated core.[5] On the other hand, the preferred processing technologies for these materials from organic solution like printing require sufficient solubility, which is usually provided by introducing solubilizing (alkyl) side-chains into oligomers and polymers or end-groups into oligomers. Although linear substituents contribute only a little to enhancing the solubility, branched equivalents are much more effective. The more bulky the substituents, the stronger the effect on solubility is. Therefore, bulky end-groups like medium-sized polystyrene (degree of polymerization 30) in an undecithiophene[6] and poly(benzyl ether) dendrons in oligo(*p*-phenylenevinylene) (OPV) gelators[7] and in oligothiophenes[8] have been described. These reports concentrate on the solution properties of the electronic materials. The improvement of processing is the focus of their application, but a weakening of the π–π interactions of the functional core as the origin for the enhancement of solubility is often overlooked. In turn, the weakening might have a strong effect on solid-state structures and thus electronic properties in (thin-film) applications. Transition-temperature engineering of liquid-crystalline oligothiophenes can be achieved by desymmetrization of the end-groups or by varying the number of methyl substituents in both branched alkyl end-groups, respectively.[9] The ordering properties of organic semi-conductors in the liquid-crystalline state is widely employed in materials science and has been described in excellent reviews.[10–13] There are some reports on the influence of the side-chain on the molecular organization and charge-transport performance of (co)polymers like diketopyrrolopyrrole-quaterthiophene copolymers (PDQTs).[14] The crystalline solid-state order of [1]benzothieno[3,2-*b*]benzothiophenes could be fine-tuned by variation of the end-groups between the bulky single-branched substituents isopropyl, *tert*-butyl and trimethylsilyl (TMS), leading to high-mobility organic semi-conductors.[15] The principle of branching in substituents by introducing silicon has been described many times in the literature but mainly for polymeric materials.[16] It can also be used to generate further topologies of the oligomers like dendrimers or multipods.[17,18] Apart from the few references described herein, there has been hardly any systematic investigation on the effect of end- or side-group structures on the solid-state properties of organic materials published in the literature. We have reported on the effect of varying branching topology on the solid-state properties of long oligothiophenes (septithiophenes and longer) with single-branched end-groups.[19–22]

The present contribution is a logical extension of the previous reports, with further branching points introduced into the substituents. In total, five new substituents were synthesized and introduced into septi-, noni- and undecithiophenes with systematic variation of the linkers between the branching points leading to dendrimer-like structures (Scheme 1). This

[a] *Institut für Organische Chemie III, Universität Ulm, Albert-Einstein-Allee 11, 89081 Ulm, Germany*
E-mail: ulrich.ziener@uni-ulm.de
http://www.uni-ulm.de/nawi/institut-fuer-organische-chemie-iii/
[b] *DWI-Leibniz Institute for Interactive Materials, Forckenbeckstrasse 50, 52056 Aachen, Germany*
Supporting information and ORCID(s) from the author(s) for this article are available on the WWW under http://dx.doi.org/10.1002/ejoc.201700046.

causes an increased competition between the bulkiness of the substituents and the π–π interactions of the oligomeric cores, which has a substantial effect on the thermodynamic properties of the oligomers in the solid state such as the total transition enthalpies and entropies and clearing temperatures. This competition is also made responsible for the appearance of liquid-crystalline phases in accordance with reports on septithiophenes with more crowded single-branched substituents compared with less-crowded substituents in the bulk and thin film.[19] For the sake of readability, the five different substituents are denoted by letters or by their carbon-linker lengths. The first number gives the linker between the thiophene core and the first branching point (linker 1), the second number describes the linker between the two branching points (linker 2) and the third denotes the hexyl end-groups (Scheme 1).

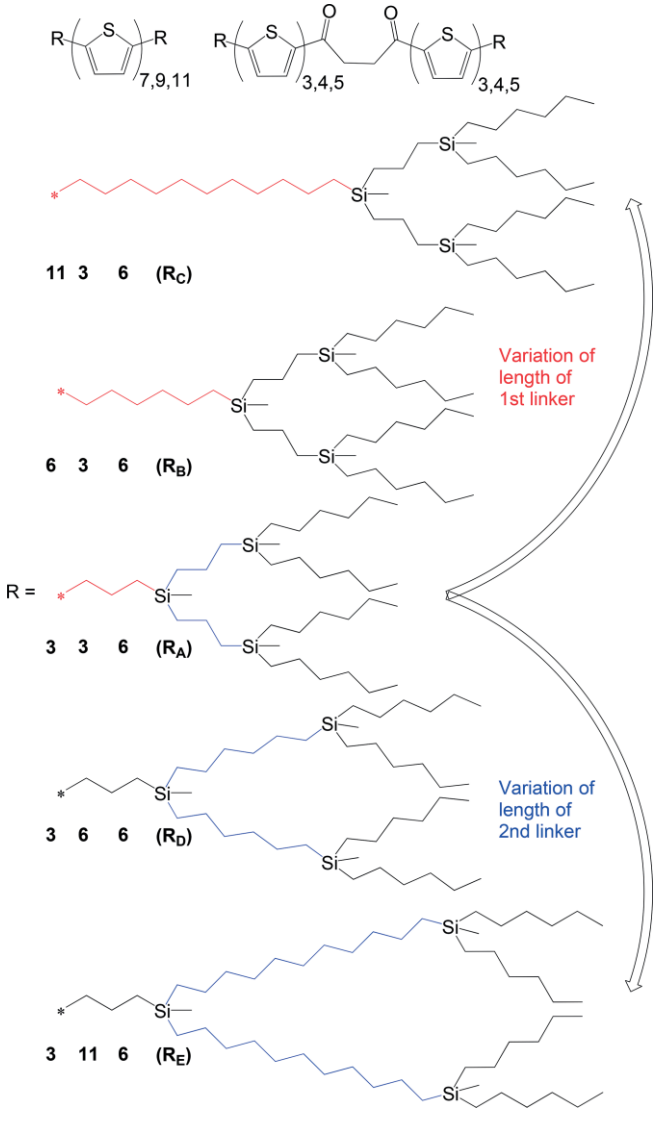

Scheme 1. Schematic structures of the oligomers and pre-oligomers and substituents with varying branching topology.

Results and Discussion

The oligomers with different branched aliphatic end-groups were synthesized by metal-catalysed coupling chemistry. At first, the various substitution patterns were prepared at a single thiophene unit (Scheme 2) followed by the construction of the oligomers (Scheme 3), similarly to a procedure previously described for oligomers with mono-branched substituents.[21,22] Thiophene was lithiated and alkylated with a bromoalkene and in a hydrosilylation step treated with dichloro(methyl)silane to give **1T*n*Si** (Scheme 2). It turned out that the usage of the quite common Karstedt catalyst did not give full control over the regiochemistry with partial formation of the Markovnikov adduct instead of the anti-Markovnikov product, which were barely separable. Therefore, we employed the literature-known N-heterocyclic carbene complex [(ICy)Pt(dvtms)][23,24] (Scheme 2), which led to the quantitative formation of the desired regioisomer. Furthermore, the catalyst reacts selectively with terminal double bonds and additions to rearranged double bonds, occasionally found for the Karstedt catalyst, were not observed for [(ICy)Pt(dvtms)]. Subsequently, the chlorine atoms were substituted with Grignard reagents generated in situ from allyl, hexenyl and undecenyl bromide to yield five different pre-substituents **1T*n*SiAlkene** (Scheme 2). Finally, the alkenyl end-

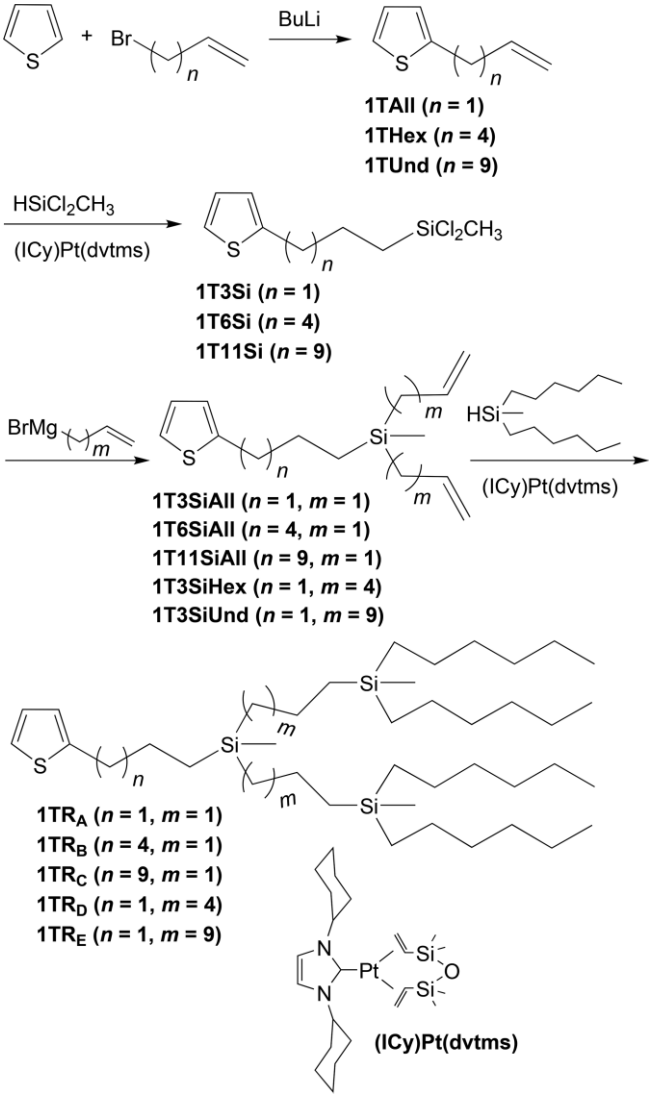

Scheme 2. Synthesis of **1TR** with the double-branched substituents R_A to R_E.

groups were hydrosilylated with dihexyl(methyl)silane to deliver the mono-substituted thiophenes **1TR** with the substituents 3–3–6 (**1TR$_A$**), 6–3–6 (**1TR$_B$**), 11–3–6 (**1TR$_C$**), 3–6–6 (**1TR$_D$**) and 3–11–6 (**1TR$_E$**) (Scheme 1 and Scheme 2). The thiophenes **1TR** were mostly obtained in reasonable overall yields of between 70 and 80 % for the various steps.

Subsequently, **1TR** was allowed to react with BuLi and MX and treated in a Stille- or Suzuki-type coupling reaction with 2-bromothiophene, 5-bromobithiophene or 5-bromoterthiophene, respectively, leading to the corresponding mono-substituted bi-, ter- and quaterthiophenes ***n*TR** (Scheme 3). Finally, the ***n*TR** oligomers were again stannylated and coupled to the diketal synthon **BrdialBr** to deliver the symmetrically substituted pre-oligomers **R*n*Tdial*n*TR**. Although the solubility of the pre-oligomers is much higher than that of the corresponding oligomers with mono-branched or even linear substituents,[25–27] it turned out that the usage of the diketal synthon (see Scheme 3) instead of plain 5,5′′-dibromoterthiophene is advantageous, especially for the substituent pattern 11–3–6 (**R$_C$**) with the long linker between the thiophene core and the first branching point. This finding is related to the solubility, which is lowest for oligomers with substituent **R$_C$**. The diketal pre-oligomers were then subjected to acidic deprotection of the diketo functionality to yield the diketo-functionalized pre-oligomers **R*n*Tdion*n*TR** and the ring-closure reaction with Lawesson's reagent to form the final septi-, noni- and undecithiophenes **R*n*TR** (Scheme 3). Although the oligomer series with all five substituents could be obtained for **R7TR** and **R9TR** after purification by column chromatography and recrystallization, the solubility of substituent **R$_C$** was again too low (see above) to prepare the corresponding undecithiophene in acceptable purity. Hence, in total 14 new oligomers were synthesized in moderate-to-good yields.

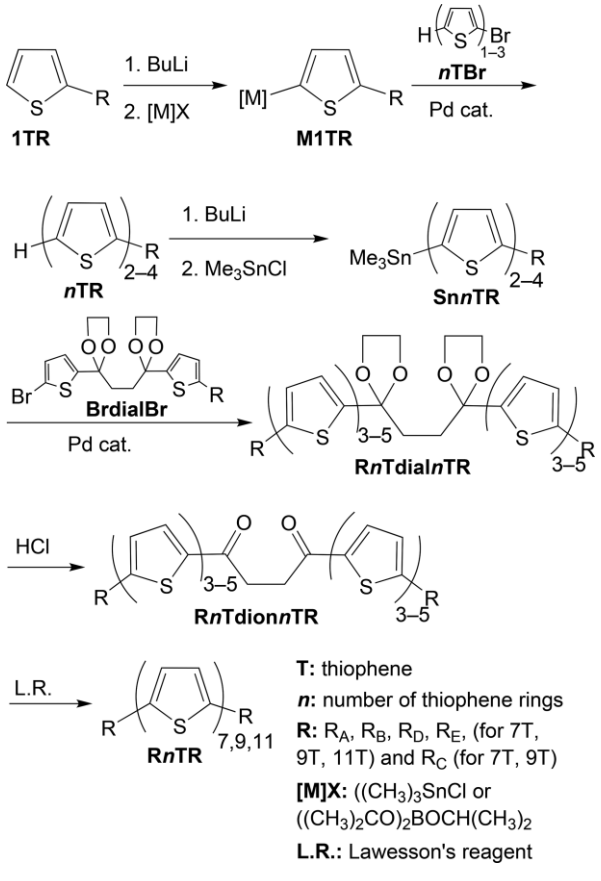

Scheme 3. Synthesis of the symmetrically substituted septi-, noni- and undecithiophenes **R*n*TR**.

All the final oligomers **R*n*TR** and the corresponding pre-oligomers **R*n*Tdion*n*TR** show multiple thermal phase transitions with variable temperature ranges depending on the structure of the substituents. All thermal data are summarized in Table S1 in the Supporting Information. Figure 1 shows exemplarily the thermogram of septithiophene **R$_A$7TR$_A$**, which will be explored more in detail (see below).

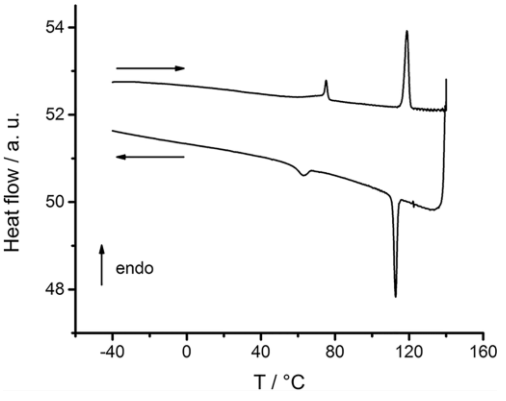

Figure 1. DSC thermogram of **R$_A$7TR$_A$** as a representative example for various series of oligothiophenes.

The behaviour observed is quite similar to the mono-branched counterparts with varying positions of the branching point reported earlier.[22] Looking at the temperatures T_c for the highest thermal transition to the isotropic phase, the two additional dihexyl(methyl)silyl groups in the present substituents cause a lowering of the thermal transition of around 40 K [e.g., T_c = 177 °C (**R′7TR′**) and 270 °C (**R′9TR′**) for R′ = $C_3H_6Si(CH_3)(C_{10}H_{21})_2$[22] vs. T_c = 138 °C (**R7TR**) and 225 °C (**R9TR**) for **R$_E$** (Figure 2)]. This is expected as the additional branching causes an increase in the volume of the branch, and thus the volume ratio *v*(branch)/*v*(linker), introduced earlier as the so-called packing parameter *P*.[22] An increasing *P* was found to decrease the intermolecular forces and thus to lower, for example, the transition temperatures. Correspondingly, it is no surprise that the temperatures T_c increase with increasing length of the linker (3 → 6 → 11) between the thiophene core and the first branching point [T_c(**R$_A$**) < T_c(**R$_B$**) < T_c(**R$_C$**)] (red filled symbols in Figure 2). The relative effect of the first branch is almost independent of the number of thiophene units, only the absolute temperatures are affected. An incremental increase in the transition temperatures of around 75–100 K per two thiophene units can be deduced regardless of the type of substituent, which is slightly lower than that found for less-branched or even linear substituents (ca. 50–60 K per thiophene unit).[27] Consequently, one would expect that for the double-branched substituents an increase in the length of the second linker between the first and second branching point [3 (**R$_A$**) → 6

($\mathbf{R_D}$) → 11 ($\mathbf{R_E}$)] should cause a decrease in the transition temperatures as the volume of the branched part of the substituent increases. In contrast, increasing the length of the second linker also leads to an increase in the isotropization temperatures T_c, although less pronounced than for the first linker (blue open symbols in Figure 2). Here, the influence of the length of the second linker decreases with increasing number of thiophene moieties and becomes almost negligible for **R11TR** (Figure 2). This means that a closer branch disturbs more efficiently the order of the oligomeric core than a branch further apart. These findings are valid not only for the oligomers **R*n*TR** but also for the mono-substituted **4TR** and even the pre-oligomers **R*n*Tdion*n*TR**, which means that these thermal properties follow a general principle, as postulated in our previous report.[22] This is also supported by the lower transition temperatures of the pre-oligomers **R*n*Tdion*n*TR** compared with the fully conjugated oligomers **R*n*TR**, because of the non-planar 1,4-diketo moieties and thus disturbed intermolecular π–π interactions of the pre-oligomers.

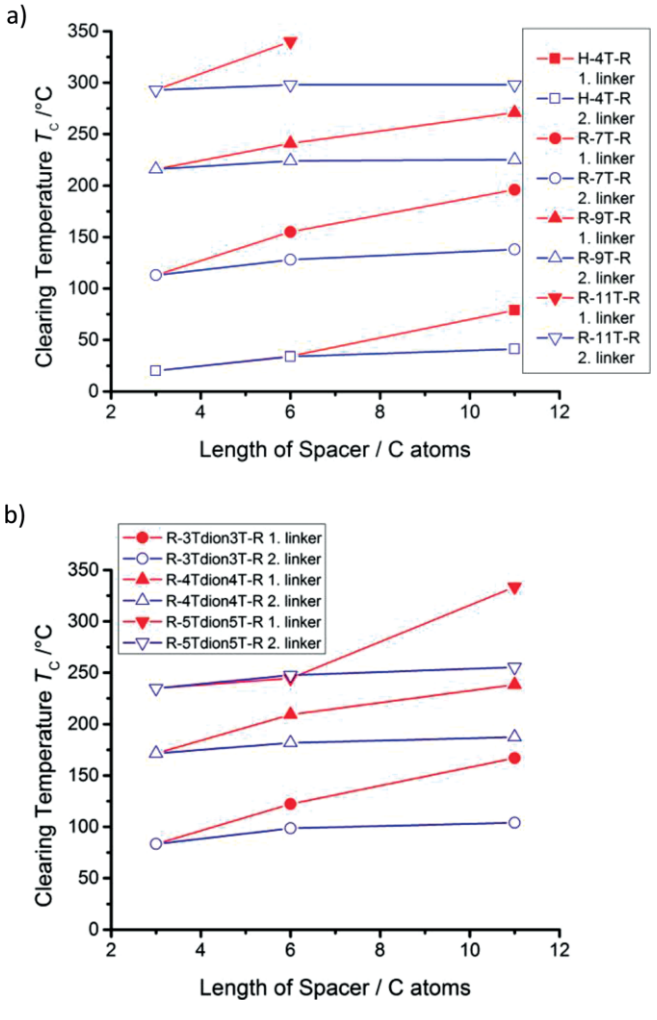

Figure 2. Clearing temperatures T_c for (a) the septi-, noni- and undecithiophenes and (b) the corresponding pre-oligomers with five different branched substituents. Red filled symbols refer to substituents $\mathbf{R_A}$, $\mathbf{R_B}$ and $\mathbf{R_C}$ and blue open symbols to $\mathbf{R_A}$, $\mathbf{R_D}$ and $\mathbf{R_E}$, respectively.

To gain more insight into the thermodynamic properties and a better understanding of the structure–property relationships we have evaluated the phase-transition enthalpies and entropies of the oligomers **R*n*TR**, pre-oligomers **R*n*Tdion*n*TR** and mono-substituted **4TR** (Figure 3). The enthalpies and entropies of all the detectable transitions between room temperature (for compounds in the crystalline state at room temp.) or lower (–50 °C for compounds in a mesophase at room temp.) and the isotropic state can be summed up regardless of the number and nature of (first-order) phase transitions according to Hess's law. The total values deliver the enthalpies and entropies for the transition between the solid-state phase with the lowest energy and the isotropic liquid phase and thus can be compared with each other on the basis of the similarity of the molecular structures. Please note that the temperature dependence of the entropy has been neglected as it will be rather minor and the data were evaluated only in comparison with similar oligomers.[28] It should be further mentioned that some of the compounds show second-order transitions (glass transitions), marked by black circles in Figure 3, characteristic of only semi-crystalline phases. Hence, the thermodynamic data might be underestimated for these compounds, but this effect should be also rather negligible in the overall evaluation as the similarities and differences in the various series are comparable regardless of the presence or absence of glassy states. The glass transitions demonstrate a strong kinetic hindrance of crystallization owing to the bulky end-groups.

The enthalpies and entropies for the **R*n*TR** series (Figure 3b–d) reveal that 1) there is only a slight increase with increasing length of the linkers, 2) the data for the first linker are always slightly smaller than for the second, 3) the length of the oligomer core plays a minor role and 4) the absolute values are surprisingly low in comparison with other α,ω-substituted oligothiophenes. The enthalpies vary between around 10 and 20 kJ mol^{-1} whereas the entropies are found between 15 and 40 J mol^{-1} K^{-1}. For comparison, the linear eicosyl substituent in a septithiophene leads to a total enthalpy of 121 kJ mol^{-1} and an entropy of 268 J mol^{-1} K^{-1}.[27] For shorter oligomers (quater- to sexithiophene) and substituents (*n*-decyl) the values are still in the range of 50 to 80 kJ mol^{-1} and 80 to 200 J mol^{-1} K^{-1} for the enthalpy and entropy, respectively.[28] Branching of the substituents causes a lowering of the values but they still amount to 33 to 48 kJ mol^{-1} and 60 to 115 J mol^{-1} K^{-1} for septithiophenes.[27] Interestingly, a small second branch, through the introduction of a 2-ethylhexyl group, reduces the enthalpy further to 20 kJ mol^{-1} and the entropy to 37 J mol^{-1} K^{-1}.[21] Hence, the much bulkier double-branched substituents in the present contribution consistently cause even lower values. This finding can be interpreted as weaker intermolecular forces in a less ordered and/or less dense packing that originates from the greater bulkiness of the substituents. This is in accordance with the minor influences of the core and linker lengths as the bulky substituents weaken the overall intermolecular interaction so effectively that additional thiophene units do not add significant attractive forces. The higher entropy gains and enthalpy losses of the heating phase transitions for the second linker compared with the first linker underline the importance of the

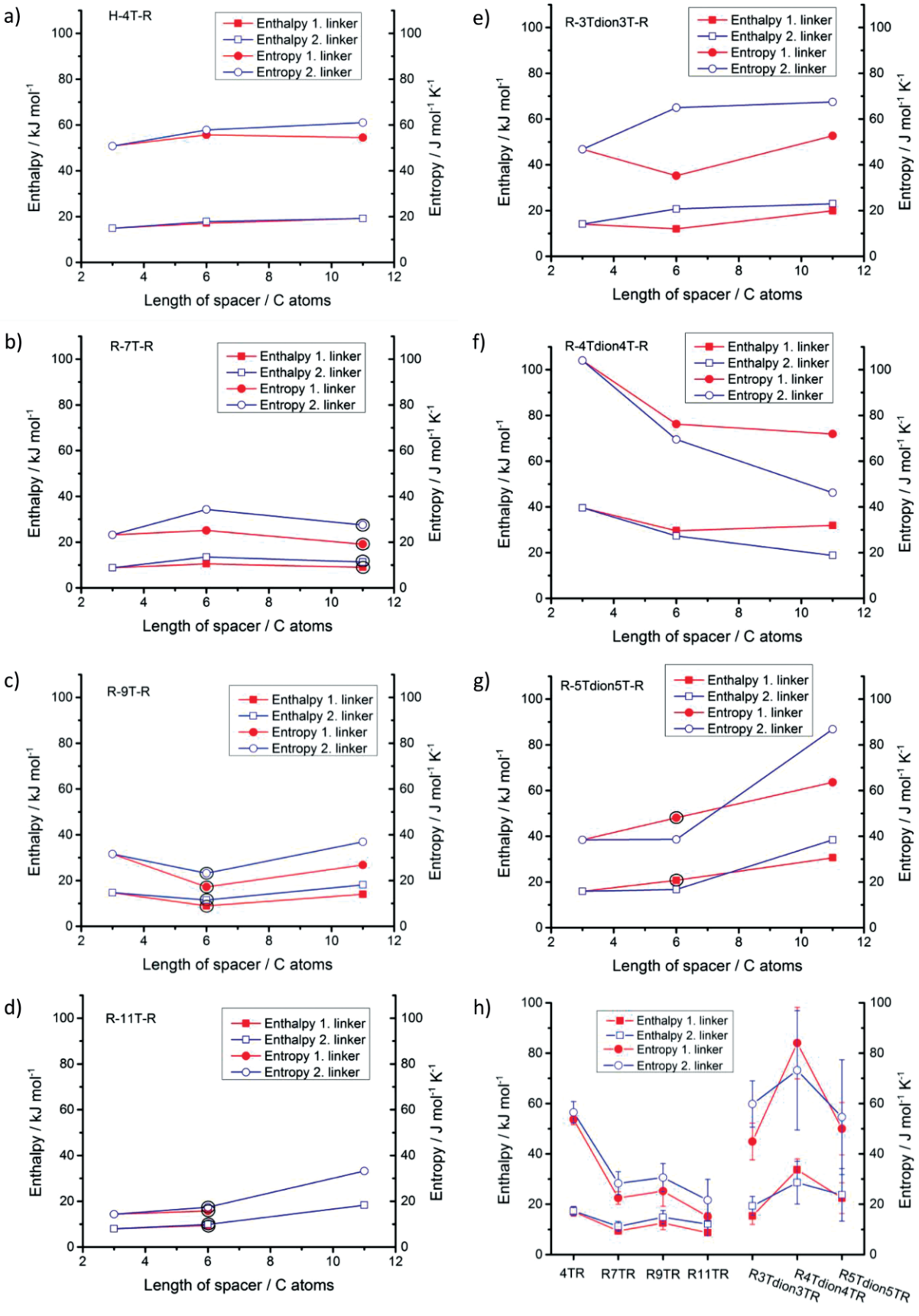

Figure 3. Sum of the phase-transition enthalpies and entropies between the lowest crystalline and isotropic liquid state for (a) **4TR**, (b–d) **R*n*TR** and (e–g) **R*n*Tdion*n*TR**. (h) Phase-transition enthalpies and entropies for the oligomers averaged over the substituents $\mathbf{R_A}$, $\mathbf{R_B}$ and $\mathbf{R_C}$ (red filled symbols) and $\mathbf{R_A}$, $\mathbf{R_D}$ and $\mathbf{R_E}$ (blue open symbols), respectively. Black circles indicate oligomers with glass transitions.

first branching point over the second one, as also found in the higher transition temperatures (see Figure 2). The values for the mono-substituted quaterthiophene (Figure 3a) are slightly larger, presumably because of the presence of just one bulky substituent compared with the **R*n*TR** series. Because of the similar transition enthalpies and entropies we have averaged the values over the different linkers for each **R*n*TR** series and the results are summarized in Figure 3h (left side).

For the pre-oligomers **R*n*Tdion*n*TR** the picture is quite different. The enthalpies and entropies are significantly larger and range from around 15 to 40 kJ mol^{-1} and from 40 to 100 J mol^{-1} K^{-1} (Figure 3e–g), respectively. Furthermore, the impact of the length of the linkers is more expressed and the trends are non-uniform. Although for **R3Tdion3TR** the values are slightly increasing, for **R4Tdion4TR** they are strongly decreasing and for **R5Tdion5TR** they are strongly increasing with increasing length of the linkers. In analogy to the oligomers **R*n*TR**, the values were also averaged over the different linkers and are displayed in Figure 3h (right side). Clearly the intermolecular forces of the pre-oligomers in the solid are stronger than for the final oligomers. This is rather surprising as the diketo unit interrupts the linear co-planar arrangement of the thiophene moieties in the core. On the other hand, it gives more flexibility to the stiff core and can thus support closer and tighter packing. Interestingly, the **R*n*Tdion*n*TR** series barely display glass transitions whereas for **R*n*TR** either $\mathbf{R_B}$ and $\mathbf{R_D}$ or $\mathbf{R_C}$ and $\mathbf{R_E}$ cause kinetically hindered crystallization (see Table S1 in the Supporting Information), which we attribute also to the lower flexibility of the fully conjugated molecules. The varying trends with increasing lengths of the linkers show a subtle dependence of the packing on the length of the core.

The overall low transition enthalpies and entropies of the final oligomers **R*n*TR** and the presence of multiple phases (see Figure 1 and Table S1 in the Supporting Information) suggest the existence of liquid-crystalline (lc) states. Indeed, temperature-dependent polarizing optical microscopy (POM) of the septi- and nonithiophene series revealed after cooling from the isotropic phase and shearing experiments fluid behaviour typical for lc phases (not shown). Similar behaviour is assumed for the undecithiophene series but the transition temperatures were too high to obtain reproducible results as the samples partially decomposed under the microscope although they proved to be stable in the differential scanning calorimetry (DSC) measurements up to the isotropic state. Figure 4 and Figure S1 (see the Supporting Information) display representative POM images with crossed polarizers of the septi- and nonithiophene series at various temperatures. The phase behaviour of the oligomers partially proves quite complex. Hence, we will focus on $\mathbf{R_A7TR_A}$ with the most easily accessible phase transitions among all the compounds (Figure 1 and Figure 4). Cooling from the isotropic phase, POM reveals clear birefringence with a fan-like texture and striation across the fans just below the onset of the high temperature transition at 112 °C (Figure 4a). The low enthalpy of around 8 kJ mol^{-1} (Figure 1 and Figure S1 in the Supporting Information) is in accordance with the fluidity of the texture upon shearing. Further cooling of the same texture region to 80 °C (Figure 4b–d) leads to a colour change of some fan domains from red to green. In the vicinity of the low-temperature transition at 65 °C (Figure 4e), straight dark lines with an angle of around 80° appear across the fans until the crystalline phase is formed below around 45 °C (Figure 4f). It can be noted that the solid at room temperature is smeary, which points to a weakly ordered crystal, potentially a soft crystal phase.[29] The textures of the mesophase are ambiguous and might indicate the presence of smectic phases,[30] presumably SmC in analogy to related oligomers in our previous investigations.[21] On the other hand, various columnar phases might show similar textures, as described in the literature.[31–34] For the other compounds of the septi- and nonithiophene series, further morphologies with maltese crosses and fern-like textures are found (see Figure S1 in the Supporting Information), which are also indicative of columnar phases. In contrast to most of our previously reported mono-branched oligothiophenes, which display almost exclusively smectic phases,[21] the bulkier double-branched substituents seem to favour the formation of columnar phases. Recently, we reported on a series of septithiophenes with increasing bulkiness and a transition from a layered structure to columnar/bicontinuous cubic in thin films.[19] The corresponding columnar structures for the present series would also be in accordance with the low values for the enthalpy and entropy, because of the reduced π–π overlap (see above).

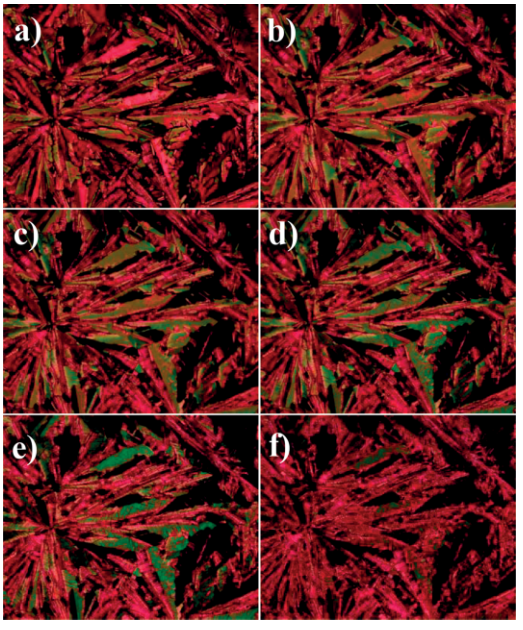

Figure 4. POM images from the same area of $\mathbf{R_A7TR_A}$ at different temperatures upon cooling from the isotropic state: (a) 112, (b) 100, (c) 90, (d) 80, (e) 65 and (f) 45 °C. The image sizes are 375 μm × 310 μm.

Based on all these arguments one is tempted to assign mainly columnar mesophases to the present oligothiophene series. However, an unambiguous assignment requires more detailed information from X-ray diffraction. We considered $\mathbf{R_A7TR_A}$, $\mathbf{R_B7TR_B}$ and $\mathbf{R_D7TR_D}$ as a series of compounds with a representative variation of structure (see Scheme 1), and typical X-ray scattering data were obtained as a function of tempera-

ture. Measuring the wide-angle X-ray scattering (WAXS) region in a reflective Bragg–Brentano geometry, the low-angle part provides basic structural information. The first data were taken for increasing temperatures and subsequently the sample was cooled from the isotropic phase, mimicking the process in POM (see Figure 4). At each measurement temperature an equilibration time of 30 min was applied. For **R_A7TR$_A$**, according to DSC and POM, a liquid-crystalline phase is expected between 112 and 73 °C (Figure 1 and Table S1). The peaks are somewhat broadened due to the relatively large beam size needed to obtain data in a reasonable time. Figure 5a gives an overview over the full *Q* range, a blow-up of the low-angle data is shown in Figure 5b. For all three compounds in the liquid-crystalline phase essentially three main peaks are observed (Figure 5c), for **R_A7TR$_A$** at Q = 1.16, 1.63 and 2.00 nm^{-1}. There is no evidence for any peaks at lower Q values.

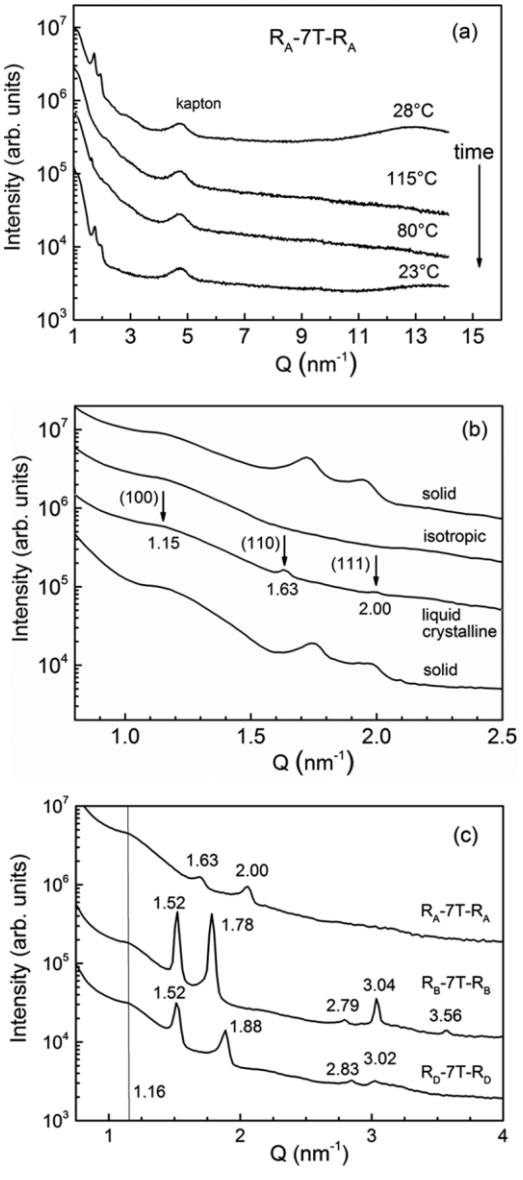

Figure 5. (a) Overview and (b) low-angle WAXS region for **R_A7TR$_A$** at various temperatures in the solid phase (23 and 28 °C), in the liquid-crystalline phase (80 °C) and in the isotropic state (115 °C). (c) Comparison of the low-angle WAXS range of the liquid-crystalline phase at 120 °C for **R_A7TR$_A$**, **R_B7TR$_B$** and **R_D7TR$_D$**.

For **R_A7TR$_A$** first we note a broad low-angle peak at around Q = 1.16 nm^{-1} corresponding to $d = 2\pi/Q$ = 5.4 nm. This value is approximately equal to the longest dimension of the molecules. This broad peak is observed in all phases, from crystalline to isotropic. Two other peaks are observed in both the solid and the liquid-crystalline phases, though at somewhat different positions. In the liquid-crystalline phase (data at 80 °C) the peak positions obey very precisely the simple ratio 1.15:1.63:2.00 = 1:√2:√3. Clearly, these results for **R_A7TR$_A$** fit a simple cubic phase (either primitive or bcc).[35]

Percec et al.[36] have reported extensively on a series of wedge-shaped mono-dendrons that self-assemble into spherical supramolecular dendrimers that form, in turn, a $Pm\bar{3}n$ 3D cubic lattice. In these cases the diameter of the dendrimer, which determines the cubic lattice spacing, is about twice the length of a wedge-shaped molecule. For **R_A7TR$_A$**, in the absence of other peaks we cannot discriminate against any of these more complicated cubic phases. In our case, the molecules have a branched end-group at each side of the thiophene core, leading rather to a dumbbell shape. We can make an analogy with wedge-shaped units and imagine the dumbbell compounds also assemble into dendrimers that are close to spherical. This would again provide an explanation for the cubic structures. However, our dendrimers are 1) expected to be less rigid and 2) to have a diameter of about the length of a single molecule, in agreement with the lowest-angle X-ray peak. The assumption of stable, but still loosely associated complexes explains the presence of the broad lowest-angle peak in all phases.

The comparison with **R_B7TR$_B$** and **R_D7TR$_D$** presents some complications. In principle, the structures of their X-ray patterns are similar to that of **R_A7TR$_A$**, with two main peaks now at slightly shifted positions. In addition, some higher orders appear. However, now the peaks do not obey the simple relation for a cubic phase, as was the case for **R_A7TR$_A$**. Nevertheless, for **R_D7TR$_D$**, they are exactly in the proportion √2:√3, but without a fit to the fundamental. The main scattering units in the molecules are the thiophene core and the Si atoms. Hence the shift in position of the two main peaks to lower Q values can in principle be attributed to the increased distance between the core and the Si atoms. Qualitatively, the following overall picture emerges. The compounds form loosely associated complexes in all phases. In the liquid-crystalline phases these assemble into cubic-like structures that are distorted/disordered such that the surface diagonal (√2) and the inner diagonal (√3) tend to be unaffected. In **R_B7TR$_B$** and **R_D7TR$_D$** in addition some new peaks develop at about Q = 2.8 nm^{-1}. This could indicate a transition to other structures as a result of increasing distortions.

Figure 6 shows results from scanning force microscopy of the surface of a bulk sample of **R_A7TR$_A$** at room temperature. First, we note in the overview terraces with step heights of 3.4 nm (Figure 6a). A detailed look at the surface of a terrace reveals a structure of elongated "bands" with a width of around 5 nm

(Figure 6b). At further magnification one can distinguish a substructure of "blobs" of about the same size. As these magnitudes agree roughly with the cubic dimension (the step height might be underestimated because of compression by the AFM tip) we associate these "blobs" with the spherical dendrimers forming the cubic structure. If we assume the dendrimer units to be still stable at higher temperatures, this would explain the persistence of the broad peak at $Q = 1.16$ nm^{-1} in the isotropic phase due to short-range structures.

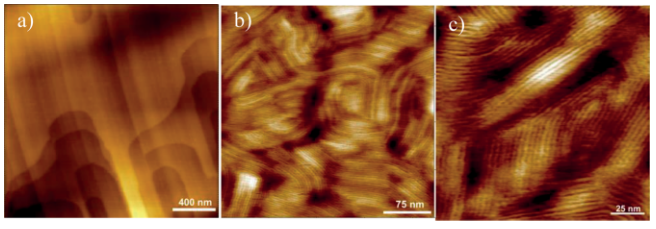

Figure 6. Scanning force microscopy images of a bulk sample of **R_A7TR_A** at room temp. (a) Overview and (b,c) detailed views.

Conclusions

We have reported on the synthesis of a highly systematic series of α,ω-substituted septi-, noni- and undecithiophenes with double-branched substituents and varying lengths of alkyl linkers. The compounds were characterized by their thermal properties and exhibit multiple phases that show a clear dependence between linker length and highest thermal transition temperature. The overall phase-transition enthalpies and entropies are surprisingly low, which points to weakly ordered solid phases. For the corresponding pre-oligomers, the values are in the expected range found in the literature for similar compounds. The thermodynamic data together with the textures from polarizing optical microscopy suggest that mainly columnar phases are formed, in contrast to the smectic phases found for oligomers with linear or mono-branched substituents. Instead, exemplary temperature-dependent X-ray data of one member of the septithiophene series reveals the presence of cubic phases. This finding is further supported by AFM investigations of the room-temperature phase. The construction of the substituents allows fine-tuning of the thermal properties and adjustment to appropriate applications, for example, molecular electronics.

Experimental Section

General: *n*-Butyllithium (2.5 M in *n*-hexane), 2-bromothiophene (98 %), succinyl chloride (95 %) (all Acros), thiophene (99+ %), dichloro(methyl)silane (99 %), Lawesson's reagent (97 %), 2-isopropoxy-4,4,5,5-tetramethyl-1,3,2-dioxaborolane (98 %), allyl bromide (99 %), trimethylstannyl chloride (97 %), 1-bromohexane (98 %), platinum(0) 1,3-divinyl-1,1,3,3-tetramethyldisiloxane (2 % in xylene), *p*-toluenesulfonic acid monohydrate (98.5 %), tetrafluoroboric acid (48 % in H_2O), $[Pd(dppf)Cl_2]\cdot CH_2Cl_2$, $[Pd_2(dba)_3]\cdot CHCl_3$, tris(*o*-tolyl)phosphine (97 %) (all Aldrich), 11-bromo-1-undecene (Alfa Aesar, 95 %), magnesium (>90 %), *N*-bromosuccinimide (>99 %), 5-hexen-1-ol (>90 %), triphenylphosphane (>99 %), ethylene glycol (>99 %), aluminium chloride (>98 %), potassium *tert*-butanolate (98 %), sodium hydrogen carbonate (99.5 %), cyclohexylamine (99 %), glyoxal (40 % in H_2O), potassium carbonate (99 %) (all Merck), $[Pd(PPh_3)_4]$ (Strem, 99 %), HCl (VWR BDH Prolabo, 37 %), sodium chloride (VWR BDH Prolabo, 99 %) and the solvents THF, acetone, ethyl acetate, ethanol, methanol, diethyl ether, *n*-hexane, toluene, dichloromethane, chloroform, petroleum ether (all VWR BDH Prolabo, GPR Rectapur), benzene (Aldrich, 99.9 %), 1,1,2,2-tetrachloroethane (Aldrich, 98 %) and DMF (Sigma, 99.9 %) were purchased and used without further purification except for reactions involving organometal species. These were performed with dry solvents under inert gas conditions. 1-Bromohexene,[37] 2-allylthiophene (1TAll),[38] 5-bromo-2,2′-bithiophene,[39] 5-bromo-2,2′:5′,2″-terthiophene,[40] 2,2′:5′,2″-terthiophene,[39] 2-(hex-5-enyl)thiophene (1THex),[21] 2-(undec-10-enyl)thiophene (1TUnd),[21] dihexyl(methyl)silane,[20,21] 1,4-bis(5-bromothien-2-yl)butane-1,4-dione,[41] 1,2-bis[2-(5-bromothien-2-yl)-1,3-dioxolan-2-yl]ethane,[25] 1,3-dicyclohexylimidazolium tetrafluoroborate[42] and Pt(*N*,*N*′-dicyclohexylimidazol-2-ylidene)(divinyltetramethylsiloxane)[24] were synthesized according to literature procedures.

^{1}H and ^{13}C NMR spectra were recorded at room temperature, unless otherwise mentioned, with Bruker AMX 400 and 500 spectrometers. All NMR measurements were carried out in $CDCl_3$ or $C_2D_2Cl_4$ with the solvent residual peak as internal reference [$CDCl_3$: $\delta = 7.24$ ppm (^{1}H) and $\delta = 77.0$ ppm (^{13}C); $C_2D_2Cl_4$: $\delta = 6.00$ ppm (^{1}H) and $\delta = 74.20$ ppm (^{13}C)]. Mass spectrometry was performed with Bruker Reflex III (MALDI-TOF), Bruker SolariX (HRMS-MALDI-FTICR) and Finnigan Mat SSQ 7000 (CI) spectrometers. UV/Vis spectra were recorded with a Perkin–Elmer Lambda 16 spectrophotometer. Elemental compositions were determined with an Elementar Vario EL instrument.

Differential scanning calorimetry (DSC) was performed with a PerkinElmer DSC 7 instrument at a heating rate of 10 K min^{-1}. Three heating and two cooling curves were measured and the thermal data were extracted from the second heating curves.

Polarizing optical microscopy (POM) images were obtained between two glass slides with a Zeiss Axioskop equipped with a Mettler FP 90 hot stage. For the shearing experiments the glass slides in the hot stage with the samples in between were sheared manually and observed under the microscope. The images are the original data without further treatment.

Wide-angle X-ray scattering (WAXS) was performed by using an Empyrean set-up from PANalytical. A copper X-ray tube (line source of 12×0.04 mm^2) provided Cu-K_α radiation with $\lambda = 0.1542$ nm. In the Bragg–Brentano geometry used, the divergent beam (divergence slit of 1/8°) was refocused at a pixel detector and recorded as a function of the scattering angle 2θ. The perpendicular divergence was restricted by Soller slits to angles ≤2.3°. Subsequently, the peak positions were calculated from $Q = 2\pi/d = (4\pi/\lambda)\sin\theta$, in which Q is the scattering vector.

Scanning force microscopy images were obtained by using a Bruker Dimension ICON instrument. The surface morphology of a thick film (the sample was a molten powder that was used to measure the X-ray diffraction data) was imaged with a scanning force microscope in tapping mode. The tapping mode imaging was performed with standard silicon cantilevers (Nano world, NCH-W point probe).

Supporting Information (see footnote on the first page of this article): Detailed information on the synthesis of the new compounds, further POM images and complete data of the thermal transitions.

Acknowledgments

We gratefully acknowledge financial support of the present work by the Deutsche Forschungsgemeinschaft (ZI567/4-3 and MO982/2-3).

Keywords: Substituent effects · Thermodynamics · Oligomers · Sulfur heterocycles · X-ray diffraction · Polarizing optical microscopy

[1] H. Sirringhaus, *Adv. Mater.* **2014**, *26*, 1319–1335.
[2] K. A. Mazzio, C. K. Luscombe, *Chem. Soc. Rev.* **2015**, *44*, 78–90.
[3] A. Facchetti, *Chem. Mater.* **2011**, *23*, 733–758.
[4] N. Thejo Kalyani, S. J. Dhoble, *Renewable Sustainable Energy Rev.* **2015**, *44*, 319–347.
[5] J. Mei, Y. Diao, A. L. Appleton, L. Fang, Z. Bao, *J. Am. Chem. Soc.* **2013**, *135*, 6724–6746.
[6] M. A. Hempenius, B. M. W. Langeveld-Voss, J. A. E. H. v. Haare, R. A. J. Janssen, S. S. Sheiko, J. P. Spatz, M. Möller, E. W. Meijer, *J. Am. Chem. Soc.* **1998**, *120*, 2798–2804.
[7] S. S. Babu, V. K. Praveen, K. K. Kartha, S. Mahesh, A. Ajayaghosh, *Chem. Asian J.* **2014**, *9*, 1830–1840.
[8] P. R. L. Malenfant, L. Groenendaal, J. M. J. Frechet, *J. Am. Chem. Soc.* **1998**, *120*, 10990–10991.
[9] J. Leroy, N. Boucher, S. Sergeyev, M. Sferrazza, Y. H. Geerts, *Eur. J. Org. Chem.* **2007**, 1256–1261.
[10] E.-K. Fleischmann, R. Zentel, *Angew. Chem. Int. Ed.* **2013**, *52*, 8810–8827; *Angew. Chem.* **2013**, *125*, 8972.
[11] J. P. F. Lagerwall, G. Scalia, *Curr. Appl. Phys.* **2012**, *12*, 1387–1412.
[12] C. Tschierske, *Angew. Chem. Int. Ed.* **2013**, *52*, 8828–8878; *Angew. Chem.* **2013**, *125*, 8992.
[13] W. Pisula, M. Zorn, J. Y. Chang, K. Mullen, R. Zentel, *Macromol. Rapid Commun.* **2009**, *30*, 1179–1202.
[14] S. Chen, B. Sun, W. Hong, H. Aziz, Y. Meng, Y. Li, *J. Mater. Chem. C* **2014**, *2*, 2183–2190.
[15] G. Schweicher, V. Lemaur, C. Niebel, C. Ruzie, Y. Diao, O. Goto, W. Y. Lee, Y. Kim, J. B. Arlin, J. Karpinska, A. R. Kennedy, S. R. Parkin, Y. Olivier, S. C. Mannsfeld, J. Cornil, Y. H. Geerts, Z. Bao, *Adv. Mater.* **2015**, *27*, 3066–3072.
[16] S. A. Ponomarenko, S. Kirchmeyer in *Silicon Polymers* (Ed.: A. M. Muzafarov), Springer, Heidelberg, **2011**, pp. 33–110.
[17] S. A. Ponomarenko, N. N. Rasulova, Y. N. Luponosov, N. M. Surin, M. I. Buzin, I. Leshchiner, S. M. Peregudova, A. M. Muzafarov, *Macromolecules* **2012**, *45*, 2014–2024.
[18] D. V. Anokhin, M. Defaux, A. Mourran, M. Moeller, Y. N. Luponosov, O. V. Borshchev, A. V. Bakirov, M. A. Shcherbina, S. N. Chvalun, T. Meyer-Friedrichsen, A. Elschner, S. Kirchmeyer, S. A. Ponomarenko, D. A. Ivanov, *J. Phys. Chem. C* **2012**, *116*, 22727–22736.
[19] W. H. de Jeu, K. Rahimi, U. Ziener, R. Vill, E. M. Herzig, P. Muller-Buschbaum, M. Moller, A. Mourran, *Langmuir* **2016**, *32*, 1533–1541.
[20] A. Kreyes, Ph. D. thesis, University of Ulm, Ulm, **2010**.
[21] A. Kreyes, S. Ellinger, K. Landfester, M. Defaux, D. A. Ivanov, A. Elschner, T. Meyer-Friedrichsen, U. Ziener, *Chem. Mater.* **2010**, *22*, 2079–2092.
[22] A. Kreyes, A. Mourran, Z. Hong, J. Wang, M. Möller, F. Gholamrezaie, W. S. C. Roelofs, D. M. de Leeuw, U. Ziener, *Chem. Mater.* **2013**, *25*, 2128–2136.
[23] I. E. Marko, S. Sterin, O. Buisine, R. Mignani, P. Branlard, B. Tinant, J. P. Declercq, *Science* **2002**, *298*, 204–206.
[24] I. Markó, S. Stérin, O. Buisine, G. Berthon, G. Michaud, B. Tinant, J.-P. Declercq, *Adv. Synth. Catal.* **2004**, *346*, 1429–1434.
[25] S. Ellinger, U. Ziener, U. Thewalt, K. Landfester, M. Möller, *Chem. Mater.* **2007**, *19*, 1070–1075.
[26] A. Kreyes, M. Amirkhani, I. Lieberwirth, R. Mauer, F. Laquai, K. Landfester, U. Ziener, *Chem. Mater.* **2010**, *22*, 6453–6458.
[27] S. Ellinger, A. Kreyes, U. Ziener, C. Hoffmann-Richter, K. Landfester, M. Möller, *Eur. J. Org. Chem.* **2007**, 5686–5702.
[28] S. Ponomarenko, S. Kirchmeyer, *J. Mater. Chem.* **2003**, *13*, 197–202.
[29] I. Dierking in *Textures of Liquid Crystals*, Wiley-VCH, Weinheim, **2003**, pp. 141–144.
[30] I. Dierking in *Textures of Liquid Crystals*, Wiley-VCH, Weinheim, **2003**, pp. 91–122.
[31] T. Cardinaels, J. Ramaekers, P. Nockemann, K. Driesen, K. Van Hecke, L. Van Meervelt, S. Lei, S. De Feyter, D. Guillon, B. Donnio, K. Binnemans, *Chem. Mater.* **2008**, *20*, 1278–1291.
[32] Z. Chen, V. Stepanenko, V. Dehm, P. Prins, L. D. A. Siebbeles, J. Seibt, P. Marquetand, V. Engel, F. Würthner, *Chem. Eur. J.* **2007**, *13*, 436–449.
[33] T. Yasuda, H. Ooi, J. Morita, Y. Akama, K. Minoura, M. Funahashi, T. Shimomura, T. Kato, *Adv. Funct. Mater.* **2009**, *19*, 411–419.
[34] C. Cuerva, J. A. Campo, P. Ovejero, M. R. Torres, M. Cano, *Dalton Trans.* **2014**, *43*, 8849–8860.
[35] W. H. de Jeu, *Basic X-ray Scattering for Soft Matter*, Oxford University Press, Oxford, **2016**.
[36] V. Percec, W.-D. Cho, G. Ungar, D. J. P. Yeardley, *J. Am. Chem. Soc.* **2001**, *123*, 1302–1315.
[37] K. Antczak, J. F. Kingston, S. J. Alward, A. G. Fallis, *Can. J. Chem.* **1984**, *62*, 829–837.
[38] Y. Zhang, C. Wang, L. Rothberg, M.-K. Ng, *J. Mater. Chem.* **2006**, *16*, 3721–3725.
[39] A. Carpita, R. Rossi, C. A. Veracini, *Tetrahedron* **1985**, *41*, 1919–1929.
[40] P. Bäuerle, F. Würthner, G. Götz, F. Effenberger, *Synthesis* **1993**, 1099–1103.
[41] V. Duchenet, C. G. Andreu, J. M. Catel, G. Coustumer, *Phosphorus Sulfur Silicon Relat. Elem.* **1996**, *118*, 117–128.
[42] W. A. Herrmann, V. P. W. Bohm, C. W. K. Gstottmayr, M. Grosche, C. P. Reisinger, T. Weskamp, *J. Organomet. Chem.* **2001**, *617*, 616–628.

Received: January 13, 2017

